

# Chapter 6

## LBLN Cos-theta Nb<sub>3</sub>Sn Dipole Magnet D20



Shlomo Caspi

**Abstract** In 1996 the LBNL D20 Nb<sub>3</sub>Sn dipole magnet reached 12.8 T at 4.4 K and 13.5 T at 1.8 K, and caught the accelerator magnet community by surprise. Not only did it achieve a record field for an accelerator dipole magnet but it also demonstrated a breakthrough in Nb<sub>3</sub>Sn conductor technology. This chapter summarizes the technical aspects of D20 development and test, addresses lessons learned, and includes suggestions relevant to developing high-field magnets for future accelerators.

### 6.1 Introduction

In the 1980s and early 1990s the US Department of Energy (DOE) considered developing magnets using Nb<sub>3</sub>Sn conductor at Lawrence Berkeley National Laboratory (LBNL) (Taylor et al. 1983, 1985). Nb<sub>3</sub>Sn, a brittle, strain-sensitive superconductor, was the only superconductor that at that time had practical current density for fields up to 16 T. It was also well understood that the next high-energy hadron collider would likely require higher operating fields well beyond the present 10 T capabilities of Nb-Ti. Prior improvements in Nb<sub>3</sub>Sn magnets had been few and progress slow, but recent results at that time had been encouraging.

D20 was a magnet set to demonstrate the technology needed for future high energy colliders by building and testing a 1 m long accelerator-quality 14 T dipole. At that time, the risk of failure using brittle Nb<sub>3</sub>Sn conductor was not totally unfounded and very real—the untested technology, untested structure, and uncommon conductor were just part of the uncharted technology so that, by the time issues were resolved, 6 years had passed. Compared with how long it took to design and build Nb-Ti magnets, such a long-extended period was beyond what was commonly expected. Also compounding the technical difficulties were differences of opinion that weighed heavily on decisions. In the end, the two coils, each a double-layer Nb<sub>3</sub>Sn coil, went beyond the 10 T “wall,” and today such technology has matured to a point where Nb<sub>3</sub>Sn magnets are included in the Large Hadron Collider (LHC)

---

S. Caspi (✉)

LBNL (Lawrence Berkeley National Laboratory), Berkeley, CA, USA

e-mail: [s\\_caspi@lbl.gov](mailto:s_caspi@lbl.gov)

© The Author(s) 2019

D. Schoerling, A. V. Zlobin (eds.), *Nb<sub>3</sub>Sn Accelerator Magnets*, Particle Acceleration and Detection, [https://doi.org/10.1007/978-3-030-16118-7\\_6](https://doi.org/10.1007/978-3-030-16118-7_6)

133

Hi-Luminosity upgrade. In hindsight, 20 years after D20, some valuable lessons from that time are still relevant.

## 6.2 Magnet Design

### 6.2.1 *Design Approach*

The design approach towards D20 (Dell’Orco et al. 1993a) was “think-outside-the-box,” a concept that followed a similar approach previously tried with a unique Nb-Ti magnet (Dell’Orco et al. 1993b). D19, a 50 mm aperture Nb-Ti dipole magnet, was built and tested as a candidate for the US Superconducting Super Collider (SSC) program. With a record field of 7.6 T at 4.4 K and 10 T at 1.9 K, that magnet specifically addressed issues of high fields and Lorentz forces. By separating the traditional concept of using self-supporting collars that combine assembly and pre-stress, D19 used thin non-supporting collars for assembly alone, leaving the functionality of pre-stress to be applied during the final structural assembly. Thin elliptical collars (with a width of 3 mm on the mid-plane) were used for coil assembly and initial alignment. Pre-stress was split between a “rings and collets” loading system and a cool-down shrinkage of aluminum shell over iron. The close proximity of the iron to the coils contributed to the dipole field, and saturation harmonics were handled by the elliptically shaped collars. Aluminum bars between the yokes controlled the final assembly.

The successful test of D19, performing without training at 4.4 K, became a model for the D20. The D20 design (Dell’Orco et al. 1995; Scanlan et al. 1995) had a considerable number of additional steps with a complexity that required an integrated design approach. A multi-phased heat treatment, thermal expansion of materials, protection heaters, epoxy impregnation, assembly, and stress pre-loading were mostly still to be understood. This chapter describes the D20 design as it was done in the early 1990s: a time when many presently available tools and programs, especially 3D, were not available or had just started to emerge. Therefore, certain design aspects, routinely used today, were missing and were not implemented in D20.

### 6.2.2 *Magnetic Design Optimization*

D20 was designed to extend accelerator magnet technology to high fields by using Nb<sub>3</sub>Sn cables with sufficient current density to deliver fields over 13 T. The graded design used two double layers with different wire and cable sizes, placing the larger strand size in the inner layer. The magnetic design underwent three successive iterations:

1. Infinite permeability, sector coils, no wedges;

2. Infinite permeability, stacked turns, and wedges;
3. Elliptical inner yoke with finite permeability, stacked turns, and wedges (the elliptical yoke was later replaced by a circular one).

In the first design the coils were modeled as circular sectors, no wedges, and the number of strands, diameter, and the Cu/non-Cu ratio optimized for both layers. This step led to a design of two double layers, eliminating the use of single layers with wide cables and a lead emerging out of the pole. The design with the field computed analytically was an attempt to maximize the central dipole field and reduce the sextupole and decapole components of the field. The initial graded two double-layer coils assumed a keystone cable, and used the same current margin and copper current density. The resulting magnet configuration had a short sample field of 14.3 T with a current of 6280 A/turn.

In the second design an infinite permeable boundary was placed 9 mm away from the coils, leaving room for a circular collar. Design variables were the number of block and turns keeping them close to a radial position in order to reduce wedges with sharp tips. The results yielded 13.15 T and 5 kA/turn; a lower field and current, respectively.

In the third design, permeable iron was used to size and shape the collar. The challenge was to reduce changes in the sextupole harmonic from low to high field. Up to 13 T that change was reduced to 1.8 units (Fig. 6.1). The thin collars placed the iron structure closer to the coils, resulting in a high transfer function of 2.22 T/kA that was only 14% lower than that with unsaturated iron.

### 6.2.3 Conductor Development

The four-layer D20 cosine-theta magnet (two double layers) was wound with two types of Rutherford cable over a 50 mm bore. The inner double layer (layers 1 and 2)

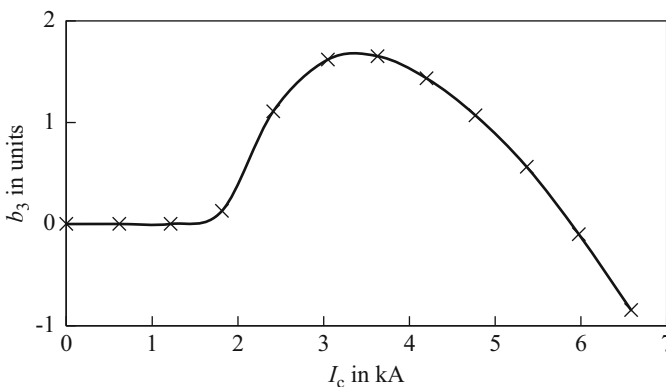
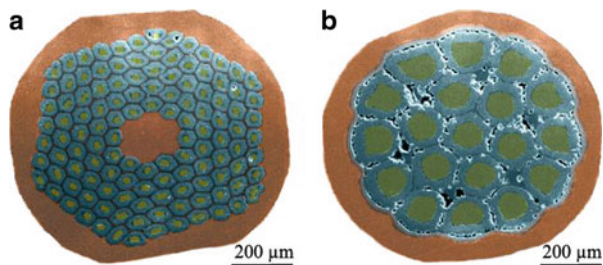


**Fig. 6.1** Sextupole variation due to iron saturation

**Fig. 6.2** Cross-sections of: (a) reacted TWCA-MJR; and (b) IGC-IT wires. (Dietterich and Godeke 2008)



used a thicker 37-strand cable with a 0.75 mm diameter strand, while the graded outer layer design used a thinner 47-strand cable with 0.48 mm diameter strand.

Two sources of  $\text{Nb}_3\text{Sn}$  wire, both based on the internal tin (IT) process, were used. The construction details of these conductors were different, although the critical currents were similar. Teledyne Wah Chang Albany (TWCA) provided a modified jellyroll (MJR)  $\text{Nb}_3\text{Sn}$  composite wire with a high volume fraction of tin, niobium, and Nb diffusion barrier in order to produce a high critical current density  $J_c$ . Intermagnetics General Corporation (IGC) provided a composite wire with a low copper to non-copper ratio, a moderately high volume fraction of niobium and tin, and a tantalum diffusion barrier. Two different wires, one for the inner layer cable and one for the outer layer cable, were ordered from each supplier. Both cables initially had a keystone cross-section with keystone angles of  $1.11^\circ$  and  $0.87^\circ$  for the inner and outer double layers, respectively. The cable cross-section was later changed to rectangular. Cross-sections of reacted MJR-TWCA and IT-IGC strands in soldered cables are shown in Fig. 6.2.

To optimize the cables' parameters, strands were extracted from the cables and their critical current was measured. In addition, the critical currents of these cables were measured as a function of applied stress, indicating a large degradation in critical current due to the cabling operation and a large dependence of critical current on the applied transverse stress. Subsequently, cables were made without a keystone and repeated tests showed little cabling degradation and improved stress dependence (Dietterich and Godeke 2008). As a result, the magnet cross-section was redesigned using rectangular cables.

Micrographs of strands removed from keystone cables showed the cause of the  $J_c$  degradation to be severe deformation of the filament bundles on the cables' narrow edge. Micrographs of strands removed from the rectangular cables showed no sheared bundles of filaments. Strands of the TWCA inner layer material still, however, showed some breaks in the niobium diffusion barriers at the edge of the rectangular cable. Since the inner strands of the IGC material did not show any breaks in the diffusion barriers, this material was chosen for the inner coils.

The geometry and final cables used in this magnet are listed in Table 6.1. The cables were insulated using a 0.12 mm thick S2-glass sleeve, which is discussed below.

**Table 6.1** D20 cable final parameters

	Inner coil <sup>a</sup>	Outer coil
Layer	1 and 2	3 and 4
Conductor type	IGC/TWCA	TWCA
Strand diameter (mm)	0.75	0.48
Cu/non-Cu ratio	0.43	1.06
Number of strands	37	47
Insulated cable width (mm)	14.66	11.88
Insulated cable thickness (mm)	1.58	1.12
Keystone angle	0	0
Twist pitch length (mm)	93.5	81.28
Residual resistivity ratio (RRR) (upper/lower coil)	201/47.5	44.9/51.6

<sup>a</sup>One of the two inner coils was made with TWCA wire

### 6.2.4 Mechanical Design and Analysis

The mechanical structure of D20 (see Fig. 6.3) was similar to that of D19. The use of elliptical collars was later abandoned as it was realized that they were unnecessary with four-layer-thick coils. The initial design considered the use of an external structural shell. This was later revised and the shell replaced by 18 layers of a rectangular stainless-steel wire wound over the yoke with a tension of 500 N. The high tension wire winding forced the yoke gap to close during cool-down. A coil pre-stress of 110 MPa on the inner layer and 90 MPa on the outer layer was needed to prevent coil separation at 13 T.

The vertically split iron yoke had a measured tapered gap that varied from 0.56 mm inside to 0.76 mm at the yoke outer radius of 381 mm. An aluminum bar, 280 mm long with a 0.25 mm clearance, was placed between the yokes to control the initial assembly and cool-down. This clearance allowed initial compression to take place during assembly and the yoke gap to close tightly during cool-down. During cool-down, the coils lost on average 11 MPa of pre-stress. When the magnet was energized to 13 T, the Lorentz force partially unloads the yoke gap without completely opening it. This approach of keeping the yoke gap closed at all times made the structure very stiff. Winding a rectangular wire around the yoke until the coil pre-stress was achieved had a real advantage compared with the alternative use of a 25 mm thick welded shell. The wire-wound method was easier and more controllable during that phase of research and development.

The mechanical analysis assumed that all materials are isotropic, linearly elastic, the coils have no hysteresis, the coils and the copper wedges are bonded, there is no friction, and the plane-stress analysis is valid. The initial coil Young's modulus was 17 GPa; it was, however, later revised according to measurements (Chow and Millos 1999) (Table 6.2). The calculated average stress distributions in the D20 design with an outer welded shell structure and an outer winding structure are shown in Tables 6.3 and 6.4. Three load cases have been examined: (a) full assembly at

**Fig. 6.3** Final cross-section: 1 – stainless-steel wire wrap; 2 – aluminum block; 3 – split yoke gap; 4 – circular spacer; 5 – coil

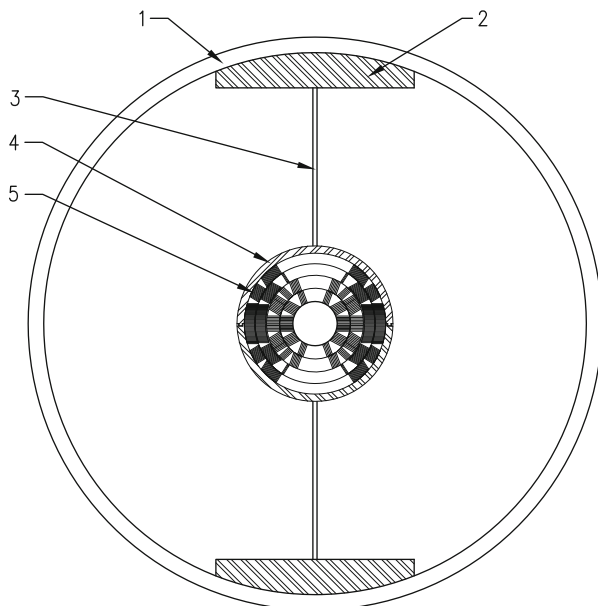


**Table 6.2** Mechanical properties of D20 coils (Chow and Millos 1999)

	$E$ modulus at 300 K measured/ calculated (GPa)	$E$ modulus at 77 K measured (GPa)	Contraction at 293– 77 K (%)
Inner coil	38/40	42	0.29
Outer coil	33/37	36	0.26

**Table 6.3** Average stress distribution in D20 design with outer welded shell structure only

	300 K	4.3 K	13 T
Mid-plane inner coil (MPa)	107	93	100
Mid-plane outer coil (MPa)	90	81	122
Pole inner coil (MPa)	109	96	25
Pole outer coil (MPa)	90	81	22
Force half gap (N/mm)	0	2826	1240
Force Al bar (N/mm)	516	0	0
Stress shell (MPa)	280	405	406

room temperature; (b) magnet cool-down to 4.2 K; and (c) a final load to a field of 13 T.

The room-temperature coil pre-stress did not change much during the cool-down. With Lorentz forces and a bore field of 13 T, the mid-plane stress on the inner coils increased by 12 MPa and on the outer coils by 56 MPa (Table 6.4). At the poles,

**Table 6.4** Stress distribution in D20 design with outer winding structure

	300 K	4.3 K	13 T
1 and 2 mid-plane (MPa)	79	65	77
3 and 4 mid-plane (MPa)	85	75	131
1 and 2 pole (MPa)	83	76	18
3 and 4 pole (MPa)	86	75	15
Outer wire wrap (MPa)	240	360	360
$F_x$ (N/mm/quad.)	–	–	5622
$F_y$ (N/mm/quad.)	–	–	–1984
$F_z$ (kN/end)	–	–	820

Lorentz forces decrease the stress on both layers by approximately 60 MPa, leaving an approximate 18 MPa residual compression on the coils. With no pole separation, the possibility of motion that may cause training was not expected. The loaded aluminum spacer between the yokes shrank considerably during cool-down, unloading completely and closing the yoke gap. When the field was raised to 13 T the yoke at the gap became partially unloaded but it did not open, thus keeping the coil displacements low. At 13 T, the radial displacement of the collar was 0.063 mm at the mid-plane and 0.058 mm at the pole.

### 6.2.5 D20 Final Design

The final magnet design was based on four layers of graded cos-theta coils, rectangular cable, a 50 mm aperture, a thin coil–yoke radial spacer, and a vertically split iron yoke supported by stainless-steel wire wrap. The final magnet cross-section is shown in Fig. 6.3 and the coil cross-section using rectangular cables is shown in Fig. 6.4. The coil parameters are given in Table 6.5.

Calculated magnet design parameters are summarized in Table 6.6. The strand short sample current density measurements went through several tests and revisions, and remained uncertain even as the magnet test commenced. At best the D20 design suggested it could reach 14 T at 4.5 K and 7 kA. While “doom and gloom” predictions persisted, they did not materialize and D20 succeeded beyond expectations.

## 6.3 Magnet Fabrication

Each double-layer coil was wound with an internal ramp in order to avoid an inter-layer splice in the high-field region (Fig. 6.5). The cable was insulated using a 0.12 mm thick S2-glass sleeve. The coils were fabricated using the wind-and-react (W&R) method following the final choice of heat treatment at 210 °C for 100 h, 340 °C for 48 h and 650 °C for 180 h, followed by vacuum impregnation with epoxy.

**Fig. 6.4** D20 final coil cross-section using rectangular cables

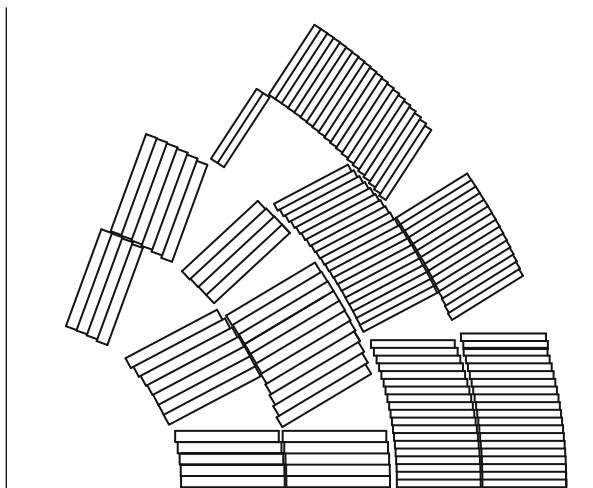


**Table 6.5** D20 coil final parameters

Layer	Inner coil		Outer coil	
	1	2	3	4
Number of turns	16	26	41	55
Number of wedges/quadrant	2	3	2	2
Inner radius (mm)	24.75	40.15	55.82	67.95
Outer radius (mm)	39.41	54.81	67.73	79.86
Coil pole corner (°)	70.56°	67.65°	57.89°	56.42°
Coil pole tilt (°)	21.16°	21.16°	35.03°	35.03°

**Table 6.6** Magnet design parameters

Parameter	Value
Magnet aperture (mm)	50
Yoke inner/outer diameter (mm)	178/762
Coil outer diameter (mm)	160
End shoe-to-shoe length (mm)	1250
Magnet end physical length (mm)	246
Magnet end magnetic length (mm)	150
Transfer function (T/kA)	2.22
Current at 13 T (kA)	6.4
Stored energy at 13 T (MJ/m)	1.1
Magnet inductance (mH)	45.6

### 6.3.1 Coil Components

The requirements for the coil component parts were metallic non-magnetic,  $E$ -modulus, and a thermal expansion coefficient matching that of the windings, and capable of surviving the reaction temperature. An aluminum-bronze alloy was



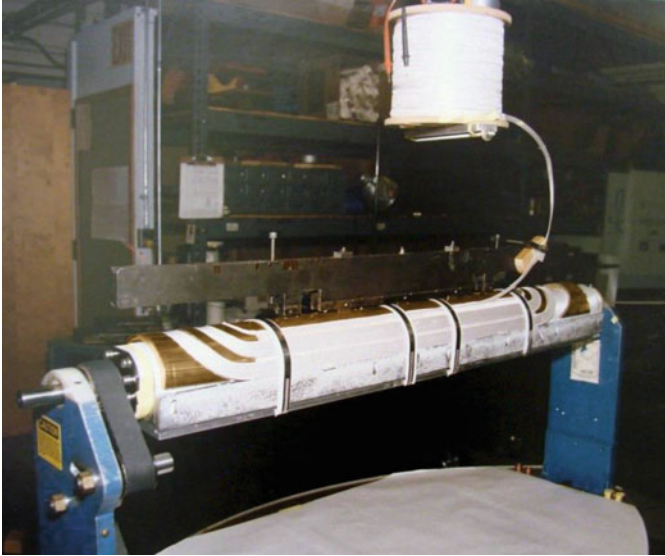


**Fig. 6.5** Split spool windings across the internal layer jump, ready to wind layer 2

chosen to meet these requirements, and several different fabrication approaches for these pieces were evaluated. Wedges were made by conventional machining, as were the pole pieces. End spacers could not, however, be machined using conventional methods due to their complex shapes.

The design of the end spacers (Fig. 6.6) was based on surface shapes according to the rulings obtained by the BEND software program (Cook 1990, 1991; Brandt et al. 1991; Caspi 1993a, 1993b; Caspi et al. 1995). Surfaces were constructed from straight lines formed by geodesic curves, which ensured minimum strain energy in the cables wound around them (Fig. 6.7). Early attempts to manufacture the spacers required the use of numerically controlled five-axis machines and data information in the form of rulings. At that time the technology was limited, and spacers were cut from machined wax cylinders and used, in a lost wax process, for casting from aluminum bronze. The casting operation proved to be very unsatisfactory, yielding parts with unacceptable tolerances and voids. A lot of handwork was required to improve the spacers' quality before they could be used in the coils. Figure 6.8 shows a selection of islands and end spacers for inner layers 1 and 2. Figures 6.9 and 6.10 show the nested turns and spacers before and after reaction. An axial cut through the inner double layer ends (Fig. 6.11) shows how turns nest as they turn over the pole. Turns near the pole clearly nest much better compared with those near the mid-plane by the shoe. Despite their distortion and de-cabing, no quenches initiated at these locations.

The technique was later improved considerably when a fully automated electrical discharge machine (EDM) became available. Shape information in the form of rulings was sent electronically to a computer-controlled EDM, which was used to

**Fig. 6.6** CAD view of layer 2 end spacers generated by the program BEND

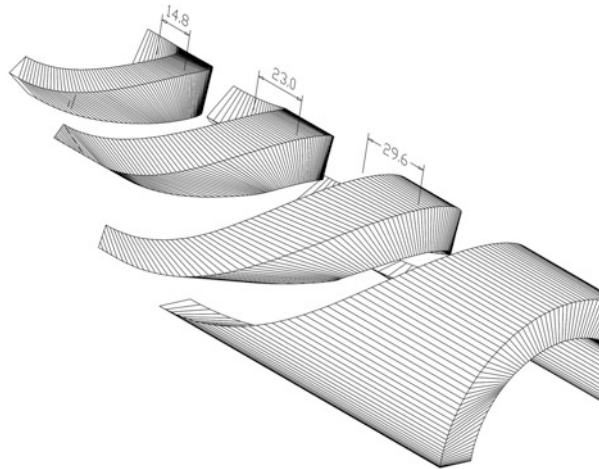


**Fig. 6.7** View of the D20 end-turn design

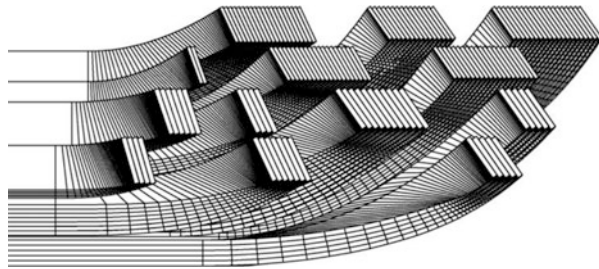


**Fig. 6.8** Layers 1 and 2 pole blocks (islands), end spacers, and saddles (shoes). White alumina coating was added to the end spacers for extra insulation

cut all the parts of a given layer from a single prefabricated bronze cylinder. This process required little human intervention, was cost-effective, and yielded high-quality parts.

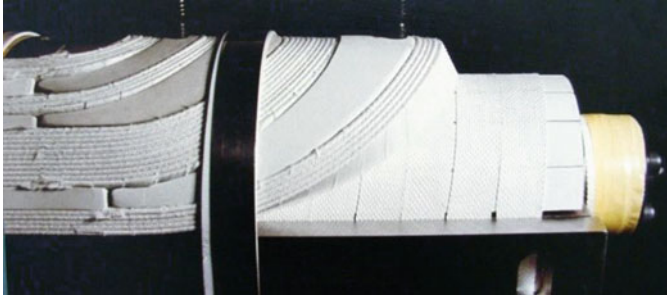


**Fig. 6.9** Layer 2 return end before reaction (end spacers coated)



**Fig. 6.10** Prototype coil with tape insulation added (note the carbon residue)

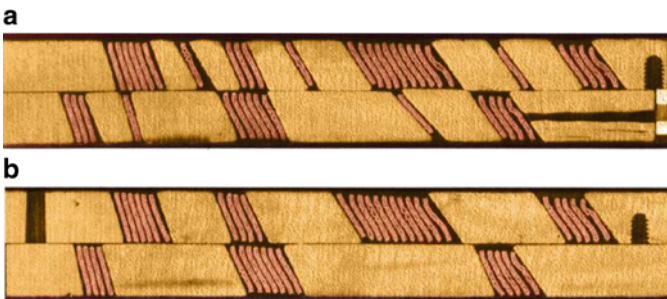


**Fig. 6.11** A longitudinal cut through (a) the inner coil lead-end; and (b) the return-end (compare with Fig. 6.7)

### 6.3.2 *Coil Insulation and Reaction*

Glass-fiber insulation was readily available. It was inexpensive and could withstand a high-temperature reaction. Initial reaction tests by the conductor manufacturers showed a somewhat surprising result. At 680 °C, the insulation remained intact and could be handled to some extent. Above 740 °C, however, the heat treatment

recommended by IGC, the insulation became extremely fragile and crumbled under the slightest handling or abrasion. Alternatives such as similar ceramic or quartz fibers were also considered, but both suffered from limited availability and relatively high cost. The solution adopted was to use a less than optimum heat treatment for the IGC conductor and keep the original glass-fiber insulation. Two types of glass-fiber insulation were evaluated: a braided tape, which was formed around the cable, and a sleeve that was made and then slipped onto the cable. The sleeve was adapted following the development of a process to show that it could be applied to a cable length of over 500 m.

The sizing used by the manufacturer left a heavy residue of carbon after reaction in an argon atmosphere. Removal of the sizing with a partial atmosphere of oxygen has been previously used in W&R Nb<sub>3</sub>Sn magnets. This approach was, however, abandoned due to problems with oxidation of the copper matrix and incomplete carbon removal in less accessible areas of the coils. Instead, the sizing was removed by pre-heating, and replaced with palmitic acid, which volatilizes in argon below 400 °C and did not leave a heavy carbon residue. A high gas flow through the coils was, however, needed to flush it from the coils. The palmitic acid was applied by dip-coating the sleeve through a solution of 1 part palmitic acid to 20 parts ethanol by weight. After dip-coating, the sleeve was passed through a drying tower to evaporate the ethanol.

Initial winding tests with the S2-glass insulation showed that occasional shorts could still be developed due to abrasion by end spacers and wedges. This problem was solved by applying a coat of plasma-sprayed aluminum oxide ceramic insulation 0.1 mm thick (Fig. 6.9). The process took some time to develop, but the ceramic coating had good adherence to the metal pieces, good bonding to epoxy, and good insulating properties.

### 6.3.3 *Splice Joints*

Each of the eight Nb<sub>3</sub>Sn leads was ramped slightly away from the mid-plane surfaces, and axially extended underneath the coil end into a low field region ( $B < 2$  T). It was then cleaned, fluxed, and sandwiched between two solder foils: Nb-Ti cables within a rectangular high purity copper box. The box was pressed towards the wide face of the cable and resistively uniformly heated until flux and excess solder flowed out both ends. The temperature was monitored to maintain reproducible splices. A typical joint took less than 2 min to fuse after initiating heating. The finished joint was insulated, mechanically supported, and vacuum-potted within the bronze end-shoe during impregnation. Typical Nb-Ti/Nb<sub>3</sub>Sn joints were measured between 0.5 and 1 nΩ at 6 T.

### 6.3.4 Coil Epoxy Impregnation

The wind-and-react (W&R) approach made it necessary for the coils to be reinforced by a combination of glass fiber and epoxy. The strength of the reinforcing matrix, in combination with the reacted Nb<sub>3</sub>Sn cable, required a series of tests to measure its mechanical properties. For this application, the epoxy had to have a low viscosity, long pot life, and be compatible with glass-fiber reinforcement. In addition, it was required to withstand cryogenic conditions. After preliminary screening, the epoxy chosen for more extensive testing was CTD-101 (Composite Technology Development, Lafayette, CO).

Both inner and outer layer cables were tested as well as samples of pure epoxy and epoxy plus glass fiber. Compression tests were performed at ambient temperature and at 77 K. Test data provided by the epoxy manufacturer were used for properties at 4.2 K. The values obtained for *E*-modulii and thermal expansion for both inner and outer cable samples are shown in Table 6.2. The values agreed well with values calculated using a rule of mixtures; the measured coefficient of expansion, however, did not. Additionally, tests were performed to find the maximum compressive load the composite stacks could withstand before the epoxy began to show cracking; loads of at least 100 MPa could be applied before the epoxy cracked. The cross-section autopsy of the four-layer impregnated coil is shown in Fig. 6.12.

### 6.3.5 Quench Protection

With a relatively high magnet inductance of 45 mH, quench protection issues had to be addressed. Protection heaters were designed to dissipate the energy over a large volume to reduce the coil's "hot-spot" temperature. These heaters were fabricated from a polyimide/stainless-steel composite sheet, and the traces were formed by a photoresist/etching process. After etching, a top sheet of polyimide was bonded to the package to produce an insulated unit 0.12–0.15 mm thick that included 0.025 mm thick stainless-steel heaters. These heater traces became bonded to the

**Fig. 6.12** D20 coil cross-section





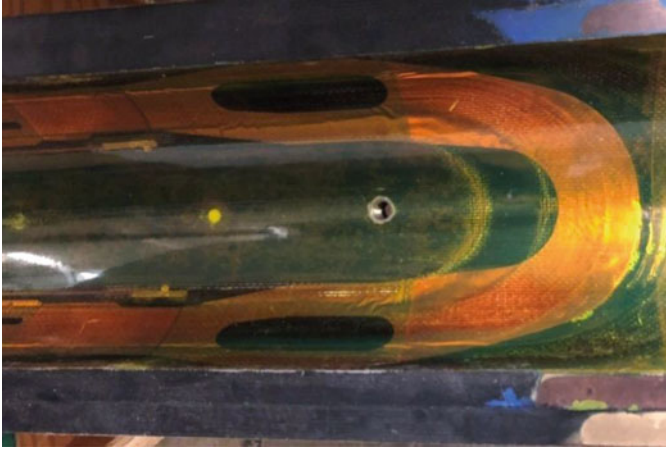


**Fig. 6.13** End view of a double-layer impregnated coil showing the end-pole, end spacer, end-shoe, and inner-layer quench protection heater

coils during the epoxy impregnation, covering over 80% of the coil turns (Fig. 6.13). With a quench detection level of 0.25 V, the temperature of the coil hot-spot was limited to less than 300 K.

### 6.3.6 Magnet Assembly

After potting, each double layer was placed back into the potting fixture, replacing one or more insulation layers on the appropriate loading surfaces with a pressure-sensitive film. The coils were then loaded to a few MPa to determine the surface profiles as well as the coil size. This sizing information along with design numbers and component measurements were used to determine the assembly details of the entire magnet. During an intermediate final assembly test, pressure-sensitive films once again replaced insulation layers on mating surfaces to check for the appropriate fit and the maximum load applied.

Initially during the first sub-assembly test the coils were placed within two aluminum-bronze half-shells and wrapped with 304 stainless-steel wires to about 50% of the calculated target tension. Pole strain gauges were used to monitor the entire operation. During the final assembly test, two yokes were placed over the bronze spacers and held together over the gap by aluminum blocks that formed a continuous circular feature.

Eighteen layers of 304 stainless steel 3 mm  $\times$  1 mm round edge wire, 14 km long were wrapped around the entire yoke assembly (Fig. 6.14). With a tension of 850 N, the stress applied to the coils was about 100 MPa and 65 MPa for the inner and outer layers, respectively. These results then led to the loading numbers of the final assembly within the yokes. End bolts held by end plates were attached to the magnet

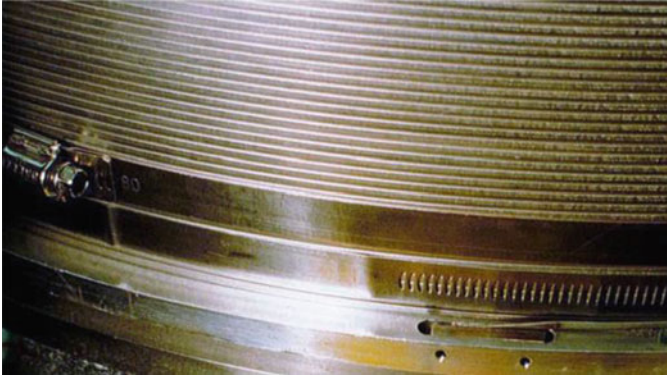


**Fig. 6.14** Close-up of the wire wrap

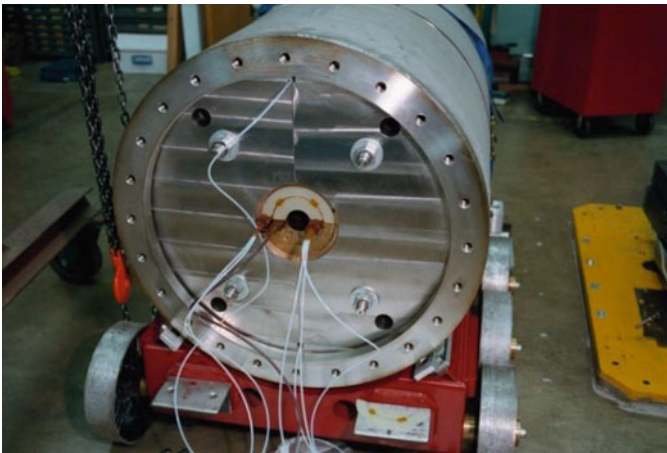


**Fig. 6.15** D20 non-lead end before installing the end plate

ends providing axial compression up to 30% of the total Lorentz force (820 kN). Bolts with pre-calibrated strain gauges were used to monitor the end force throughout the assembly and testing. Figure 6.15 shows D20 during the final assembly placed on a delivery cart.

Part theory and part reality, it turned out that during the applied pre-stress by the outer wire wrap the gap between the yokes did not remain parallel, and closed, first near the outer diameter (OD) (near the wire wraps). That required a revision of the yoke interfaces to be tapered, with a larger gap near the OD, as mentioned above. Controlling the way the iron acted during assembly and cool-down remained difficult and resulted in only partial closing of the yokes. The impact therefore was uncertainty of the coils' pre-stress.

## 6.4 Test Results and Discussion

The D20 magnet was tested at the LBNL test facility in a horizontal cryostat with an ambient pressure of liquid helium at 4.4 and 1.8 K (Fig. 6.16). The facility used an external dump resistor to reduce the stored energy absorbed by the magnet coils during a quench.

### 6.4.1 Training and Operation

The magnet was heavily instrumented with voltage taps and strain gauges. The first quench originated in the layer 1 pole at a bore field of 10.2 T. It was then followed by 13 quenches before reaching 11.34 T (Fig. 6.17, cy1). The rate of training improved when the magnet was cooled to 1.8 K, immediately raising the quench field by 9% to 12.3 T (cy1). Prior to the D20 test such jumps were seen in Nb-Ti magnets (Gilbert et al. 1989). Upon a warm-up cycle (cy2) the magnet retained a quench level of 11.9 T, and a second thermal cycle (cy3) resulted in the highest field achieved.



**Fig. 6.16** LBNL personnel during the first cycle of D20 testing. The sign reads “D20 Magnet a World Record Dipole Field of 13.3 T Reached at LBNL on March 13 1997.” The highest field record was later revised to 13.5 T as the test continued



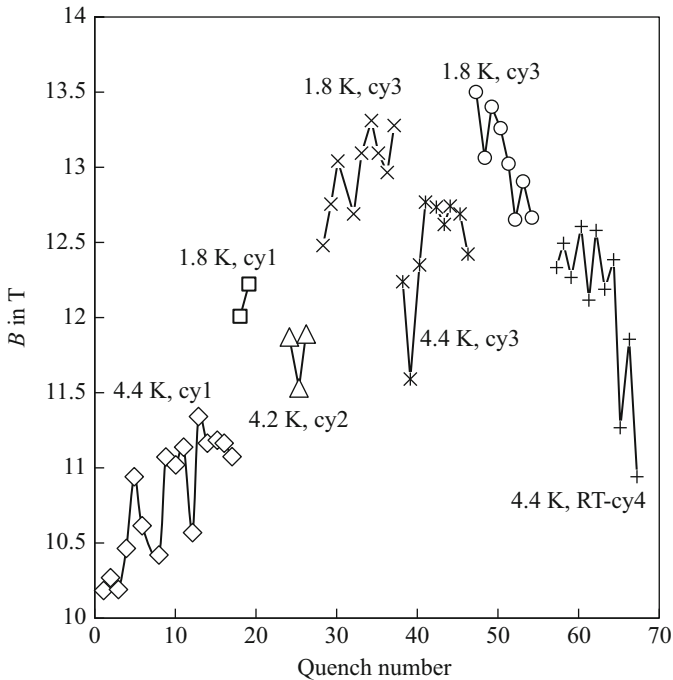


**Fig. 6.17** D20 training history

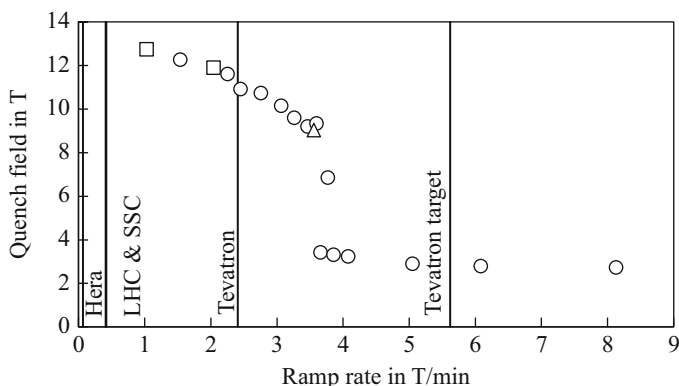
Out of the first 65 training quenches, 17 originated in layer 1, 2 in layer 2, 6 in layer 3 and 15 in layer 4 (at the low field ramp). Most quenches started at the pole turn, with later inner-layer quenches originating in the ramp region between the layer 1 and 2 poles. Six quenches originated somewhere between the pole and mid-plane. Only one quench originated in the end region. The mid-plane quenches that were anticipated from conductor degradation under the accumulated Lorentz load (130 MPa expected) never materialized. A full thermal cycle to 300 K and cool-down was also completed. Although there is considerable doubt that there was enough pre-stress when the magnet was cold, the basic mechanical structure was apparently adequate for 13.5 T. A more detailed description of test results can be found in Lietzke et al. (1997), McInturff et al. (1997), Scanlan et al. (1997) and Benjegerdes et al. (1999).

From the training curve (Fig. 6.17), D20 reached a 12.8 T limit at 4.4 K. Data suggested that the onset of this quench was thermally triggered (no spike as the quench started) indicating a possible higher limit, perhaps as high as 13.1 T.

At 1.8 K, D20 reached 13.5 T followed by a continuous slow and unstable quench performance suggesting a potential problem in the low field splice ramp of layer 4 (Fig. 6.17, cy4). This ramp had been modified before reaction in order to adjust for some earlier conductor damage. The modification is believed to have compromised the cable mechanical support, causing the quench to start with a major voltage jump

**Table 6.7** D20 highest values reached during testing

	IGC/TWCA (inner)		TWCA (outer)	
	4.35 K	1.8 K	4.35 K	1.8 K
$I_{\max}$ (A)	6300	6712	6300	6712
$B_{\text{bore}}$ (T)	12.8	13.5	12.8	13.5
$B_{\text{coil}}$ (T)	13.1	13.8	10.3	10.8
$J_{\text{non-Cu}}$ (A/mm <sup>2</sup> )	550	587	1528	1527
$J_{\text{Cu}}$ (A/mm <sup>2</sup> )	1283	1367	1441	1535

**Fig. 6.18** Ramp rate dependence at 4.4 K. Circles mark ramps starting at zero current; squares and triangles mark those started at a higher current

and then propagating very slowly before entering the high-field region. Due to the limitation in the layer 4 field ramp, training was terminated. An autopsy following disassembly showed that part of the mid-plane structure at that location did indeed collapse. It was not clear whether the conductor near the joint has been damaged irreversibly.

The highest values reached during D20 testing at 4.35 and 1.8 K are summarized in Table 6.7.

Protection heaters were generally fired with the smallest possible delay after a quench was detected, using a nominal power of 25–30 W/cm<sup>2</sup>. The measured average temperature rise was either 120 K (inner coil quench), or 185 K (outer coil quench). Typically, quench integrals of 4.3 million A<sup>2</sup>s (MIITS) were absorbed following a 13 T quench.

The ramp-rate sensitivity of D20 was measured at 4.4 K and the results compared with the required ramp-rates limits of Nb-Ti magnets of past projects (Hadron-Elektron-Ring-Anlage, LHC, Tevatron) (Fig. 6.18). Below 1 T/min the magnet was insensitive to the ramp rate, but at 3.5 T/min the field dropped abruptly from a maximum of 9 T to 3 T. We speculate that overcoming an inter-strand voltage threshold caused the sharp decline in quench current as the coil cooling transitioned from nucleate to film boiling.

### 6.4.2 Magnetic Measurements

The transfer function (Fig. 6.19) was measured with both a Hall probe and a rotating coil. Hall probe measurements were made at 8 A/s going up and 16 A/s going down. The spread in the current ramp-up vs. ramp-down measurements due to conductor magnetization is significantly reduced above 7 T. At low field of 1 T the up vs. down ramp reaches 10% with an average of 2.33 T/kA. We have checked and verified that the source of undulation in the transfer function measurements arises from the characteristics of the Hall probe and may be due to a non-linear response.

The D20 harmonics were measured with two rotating-coil systems. A 6 Hz rotating “Morgan coil” ( $R = 10$  mm,  $L = 460$  mm), placed at the radial and axial center of the magnet, measured the direct field harmonics  $b_n$  and  $a_n$  (for  $n = 1, 2, 3$ ) during a stepped power cycle up to 2 T. A wait period of several minutes was imposed after the field was changed to a ramp rate of 1 T/min to allow the harmonics to settle to steady values before measurements were recorded. A second system used a tangential and dipole-bucking coil set ( $R = 11.2$  mm,  $L = 424$  mm,  $f = 1$  Hz), for time-dependent measurements that were integrated from the magnet center through its lead end. Both the tangential and bucked signals were integrated and sampled.

The field in the magnet straight section is represented in terms of harmonic coefficients defined by the expansion

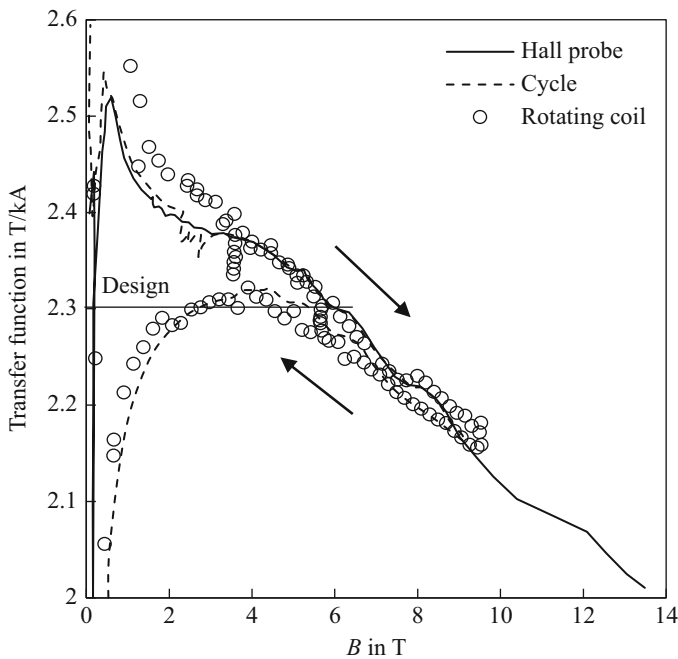


**Fig. 6.19** D20 measured transfer function vs. the bore field. The horizontal line is the computed bore field value without the coil magnetization effect

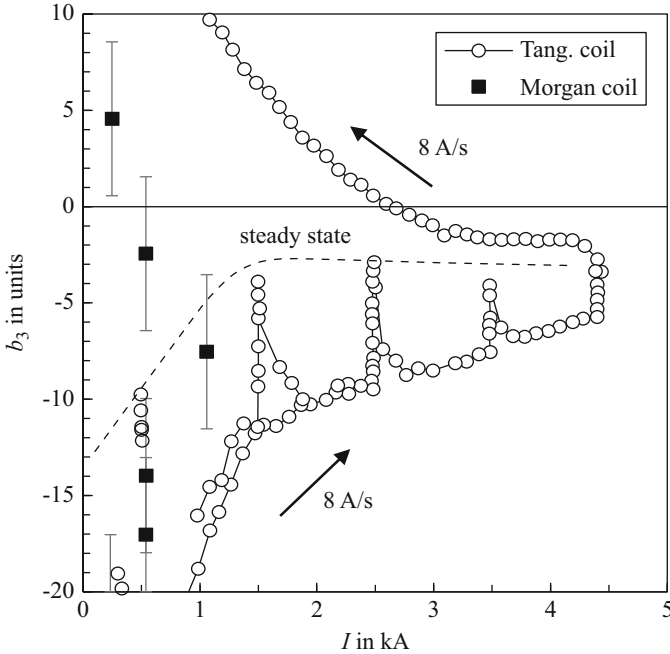


**Fig. 6.20** Measured sextupole vs. the current at low field

$$B_y + iB_x = B_1 \sum_{n=1}^{\infty} (b_n + ia_n) \left( \frac{x + iy}{R_{\text{ref}}} \right)^{n-1}$$

where  $B_x$  and  $B_y$  are the horizontal and vertical transverse field components,  $B_1$  is the dipole field component, and  $b_n$  and  $a_n$  are the  $2n$ -pole coefficients at a reference radius  $R_{\text{ref}} = 10$  mm.

The normal sextupole  $b_3$  expressed as “units” ( $10^{-4}$  of the main field component) is plotted in Fig. 6.20. Up to 10 T the sextupole  $b_3$  is quite small, approaching an asymptotic value of 4 units. All higher order harmonics were measured to well below 0.5 units except for the non-allowed skew quadrupole  $a_2$ , which was measured at 2.5 units.

### 6.4.3 Discussion

The successful test of D20 and the record field it achieved revealed several important points that suggested a potential use and improvements of  $\text{Nb}_3\text{Sn}$  technology in future high-field accelerator magnets.

- The iron yoke closed prematurely during cool-down, thereby yielding a lower cold pre-stress;
- Initial training was slow but was accelerated substantially when the magnet was cooled to 1.8 K;
- Neither the IGC nor TWCA wires seemed as stress-sensitive as short sample tests had predicted;
- Cooling was sufficient to operate at 12.5 T and 2 K when a steady-state heat input of 24 W was applied by the distributed quench heater on the inner edge of layer 1 or the outer edge of layer 2 of one coil;
- Ramp-rate sensitivity was exceptionally low for a W&R impregnated magnet;
- Except for one low field ramp, the magnet was very robust, withstanding 60 quenches above 10 T, with 37 quenches above 12 T, including a second thermal cycle;
- The magnet could be protected despite its relatively high quenching current density in the copper,  $J_{Cu} = 1535 \text{ A/mm}^2$ .

The favorable performance of D20 did not, however, erase the previous concerns about Nb<sub>3</sub>Sn magnets. The magnet design and construction was long and time-consuming due to the brittle nature of Nb<sub>3</sub>Sn, and resulted in a sense of a need for a future change by trying something other than a cosine-theta cross-section. Following the D20, two other types of magnet cross-section were built and tested at LBNL (Chiesa et al. 2003): the common coil and the window frame block. Both were explored to determine if a simpler geometry and construction technique and strain management might lead to reduced training and offset the conductor cost. As of the time of writing (2018), the gain in field has been less than 2 T and new attempts are being made to reconsider a cos-theta design like D20.

Following the thermal cycle D20 was used to provide a background field to test an insert Nb<sub>3</sub>Al cos-theta dipole constructed by The High Energy Accelerator Research Organization and Japanese industry (Wake et al. 1997). The insert coil was placed snugly within the D20 bore. During the test D20 could be held at 12.5 T, 4.4 K for an extended period (hours) without quenching. After warm-up the Nb<sub>3</sub>Al insert could not be removed without taking the D20 magnet apart. The insulation between the insert and D20 was left with deep imprint marks, suggesting the insert acted as a ridged bore supporting D20 as it tried to go elliptical.

Following the D20 test, recommendations and suggestions made by members of LBNL design team remain part of the lessons learned (not implemented):

- "...Proposals considered using D20 as a background field for testing small sample coils. A test facility capable of measuring short-sample at the 13 T level would have been, at that time, complementary to CERN's 10 T FRESCA-I test facility."
- "...Repair or replace the outer coil, re-assemble with a larger iron gap (to reduce cool-down pre-stress loss), and install it in a permanent Dewar."
- "...The magnet reached a 4.4 K limit below the expected wire short-sample value (1500 A/mm<sup>2</sup> at 12 T and 4.4 K). For a magnet like D20 to reach 16 T the current density would have to be doubled (3000 A/mm<sup>2</sup> at 12 T). With today's conductor,

this may not be as difficult as it appears. Recent short-sample tests on newly available Nb<sub>3</sub>Sn wire have delivered such non-copper current densities.”

## 6.5 Conclusion

It has been close to 25 years since the D20 program. My personal perspective following that period is that one magnet test does not tell all of the story. We should also equally recognize successes and failures and learn from both before a design changes course. The present current density of Nb<sub>3</sub>Sn composite wires is now available beyond 3000 A/mm<sup>2</sup> at 12 T. As already suggested at that time, a magnet like D20 made with today’s conductor could reach a central field above 16 T. Figure 6.21 extends D20 load lines of the central dipole field (circle) and the maximum field at the conductor (square) to a short sample of today’s conductor ( $J_{sc} = 3000$  A/mm<sup>2</sup> at 12 T and 4.2 K).

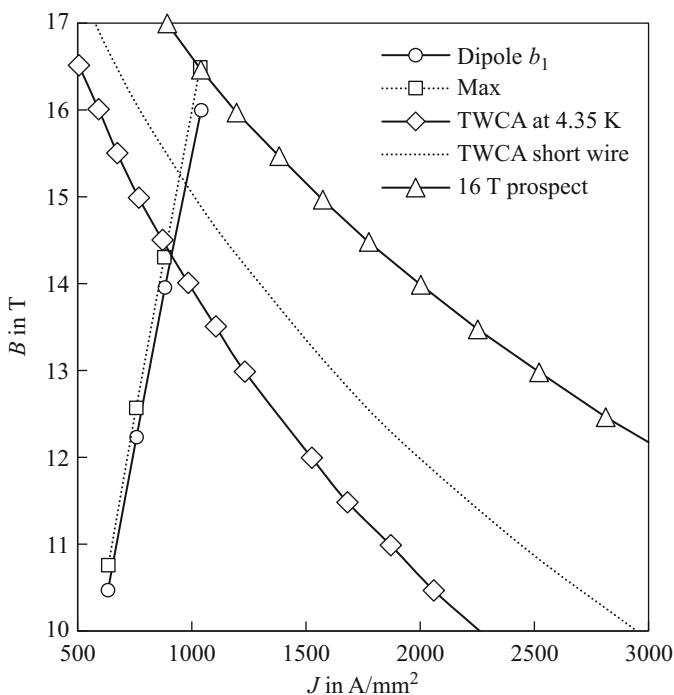


**Fig. 6.21** By extending D20 load lines and using today’s high  $J_c$  Nb<sub>3</sub>Sn wires D20 could reach a central field over 16 T

## References

- Benjegerdes R, Bish P, Caspi S et al (1999) Operational characteristics, parameters, and history of a (13T) Nb<sub>3</sub>Sn dipole. In: Luccio A, MacKay W (eds) Proceedings of the 1999 particle accelerator conference (Cat. No.99CH36366). New York, 27 Mar–2 Apr 1999, vol 5. IEEE, Piscataway, pp 3233–3235
- Brandt JS, Bartlett NW, Bossert RC et al (1991) Coil end design for the SSC collider dipole magnet. In: Conference record of the 1991 IEEE particle accelerator conference, vol 4. San Francisco, 1991, pp 2182–2184
- Caspi S (1993a) Conceptual end design of dipole D20. LBNL SC-MAG-424. Lawrence Berkeley National Laboratory, Berkeley
- Caspi S (1993b) End design of dipole D20—version d. LBNL, SC-MAG-430. Lawrence Berkeley National Laboratory, Berkeley
- Caspi S, Dell’Orco D, Ghiorso WB et al (1995) Design and fabrication of end spacers for a 13 T Nb<sub>3</sub>Sn dipole magnet. *IEEE Trans Appl Supercond* 5(2):1004–1007. <https://doi.org/10.1109/77.402720>
- Chiesa L, Caspi S, Coccoli M et al (2003) Performance comparison of Nb<sub>3</sub>Sn magnets at LBNL magnet. *IEEE Trans Appl Supercond* 13(2):1254–1257. <https://doi.org/10.1109/tasc.2003.812651>
- Chow KP, Millos GA (1999) Measurements of modulus of elasticity and thermal contraction of epoxy impregnated niobium-tin and niobium-titanium composites. *IEEE Trans Appl Supercond* 9(2):213–215. <https://doi.org/10.1109/77.783274>
- Cook JM (1990) An application of differential geometry to SSC coil end design. SSC Laboratory SSCL-N-720, Fermilab TM-1663 internal report
- Cook JM (1991) Strain energy minimization in SSC magnet winding. *IEEE Trans Magn* 27(2):1976–1980. <https://doi.org/10.1109/20.133592>
- Dell’Orco D, Scanlan RM, Taylor CE (1993a) Design of the Nb<sub>3</sub>Sn dipole D20. *IEEE Trans Appl Supercond* 3(1):82–86. <https://doi.org/10.1109/77.233677>
- Dell’Orco D, Caspi S, O’Neill J et al (1993b) A 50 mm bore superconducting dipole with a unique iron yoke structure. *IEEE Trans Appl Supercond* 3(1):637–641. <https://doi.org/10.1109/77.233783>
- Dell’Orco D, Scanlan RM, Taylor CE et al (1995) Fabrication and component testing results for a Nb<sub>3</sub>Sn dipole magnet. *IEEE Trans Appl Supercond* 5(2):1000–1003. <https://doi.org/10.1109/77.402719>
- Dietderich DR, Godeke A (2008) Nb<sub>3</sub>Sn research and development in the USA—wires and cables. *Cryogenics* 48(7–8):331–340. <https://doi.org/10.1016/j.cryogenics.2008.05.004>
- Gilbert WS, Althaus R, Benjegerdes R et al (1989) Training of LBL-SSC model dipole magnets at 1.8 K. In: Proceedings of the 1989 IEEE particle accelerator conference on accelerator science and technology, vol 3. Chicago, pp 1780–1782
- Lietzke AF, Benjegerdes R, Caspi S et al (1997) Test results for a Nb<sub>3</sub>Sn dipole magnet. *IEEE Trans Appl Supercond* 7(2):739–742. <https://doi.org/10.1109/77.614609>
- McInturff AD, Bish P, Benjegerdes R et al (1997) Test results for a high field (13 T) Nb<sub>3</sub>Sn dipole. In: Comyn M, Craddock MK, Reiser M et al (eds) Proceedings of the 1997 particle accelerator conference (Cat. No.97CH36167), Vancouver, 12–16 May 1997, vol 3. IEEE, Piscataway, pp 3212–3214
- Scanlan RM, Dell’Orco D, Taylor CE et al (1995) Fabrication and preliminary test results for a Nb<sub>3</sub>Sn dipole magnet. *IEEE Trans Appl Supercon* 5(2):1000–1003. <https://doi.org/10.1109/77.402719>
- Scanlan RM, Benjegerdes RJ, Bish PA et al (1997) Preliminary test results of a 13 Tesla niobium tin dipole. In: Rogalla H, Blank DHS (eds) 3rd European conference on applied supercon. Netherlands, EUCAS-97, 30 Jun–3 Jul 1997, Konigshof, The Netherlands. Institute of Physics Publishing, Bristol, Philadelphia, 158(2):1503–1506

- Taylor C, Meuser R, Caspi S et al (1983) Design of a 10-T superconducting dipole magnet using niobium-tin conductor. *IEEE Trans Magn* 19(3):1398–1400. <https://doi.org/10.1109/tmag.1983.1062261>
- Taylor C, Scanlan R, Peters C et al (1985) A Nb<sub>3</sub>Sn dipole magnet reacted after winding. *IEEE Trans Magn* 21(2):967–970. <https://doi.org/10.1109/tmag.1985.1063680>
- Wake M, Jaffery TS, Shintomi T et al (1997) Insertion Nb<sub>3</sub>Sn coils for the magnet development. In: Liangzhen L, Guoliao S, Luguang Y (eds) *Proceedings of the 15th international conference on magnet technology*, Beijing, 20–24 Oct 1997. Science Press, Beijing, pp 103–106

**Open Access** This chapter is licensed under the terms of the Creative Commons Attribution 4.0 International License (<http://creativecommons.org/licenses/by/4.0/>), which permits use, sharing, adaptation, distribution and reproduction in any medium or format, as long as you give appropriate credit to the original author(s) and the source, provide a link to the Creative Commons licence and indicate if changes were made.

The images or other third party material in this chapter are included in the chapter's Creative Commons licence, unless indicated otherwise in a credit line to the material. If material is not included in the chapter's Creative Commons licence and your intended use is not permitted by statutory regulation or exceeds the permitted use, you will need to obtain permission directly from the copyright holder.

